Chapter 9
Bending of Light by Gravity

To this point we have examined how massive objects move under the influence of gravity. Einstein taught us that light's motion is affected by gravity as well. Despite being relativistic, gravitational light bending can be studied with a quasi-Newtonian framework to obtain a new way to probe mass in the universe.

9.1 Principles of Gravitational Lensing

The gravitational deflection of light can be treated as a variant of the Newtonian one-body problem. A full relativistic analysis gives a deflection angle that is twice as large (see Sect. 10.6.5), but for most astrophysical purposes we can insert the factor of 2 by hand and proceed in the Newtonian framework. In this section we identify observable effect of light bending including distortion, magnification, and multiple imaging.

9.1.1 Gravitational Deflection

Consider a particle of mass m passing near a massive body $M \gg m$. The particle's trajectory is curved, but asymptotically (i.e., far from M) it is a straight line. We can quantify the bending in terms of the angle $\hat{\alpha}$ between the asymptotic segments, as shown in Fig. 9.1. To compute $\hat{\alpha}$, strictly speaking we need to solve a differential equation characterizing the motion.[1] If the bending is small, however, we can obtain a good approximation much more simply, by computing the change in velocity perpendicular to the original motion.

[1] This is related to the analysis in Sect. 3.1, but now applied to an unbound orbit.

C. Keeton, *Principles of Astrophysics: Using Gravity and Stellar Physics to Explore the Cosmos*, Undergraduate Lecture Notes in Physics, DOI 10.1007/978-1-4614-9236-8_9,

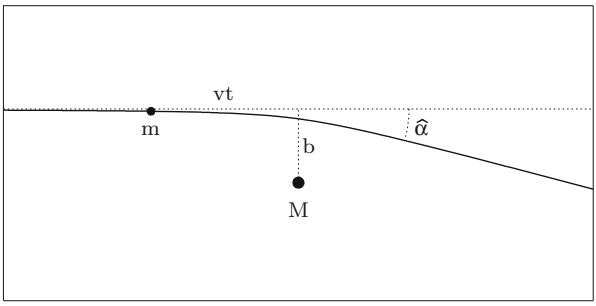

Fig. 9.1 Setup for calculating the deflection when a particle of mass m passes near a massive body M. The particle moves from left to right, and we define $t = 0$ to be the time at the point of closest approach on the original trajectory. The position shown has $t < 0$

Let the particle's speed be v. Consider the point of closest approach on the original trajectory: let the distance of this point from M, known as the **impact parameter**, be b; and let the time at this point be $t = 0$. The component of the force equation perpendicular to the (original) direction of motion is then

$$m\,\frac{\mathrm{d}v_\perp}{\mathrm{d}t} = \frac{GMm}{b^2 + v^2t^2}\,\frac{b}{(b^2 + v^2t^2)^{1/2}}$$

The first factor is the strength of the gravitational force, while the second factor gives (by trigonometry) the component in the perpendicular direction. The net change in the component of velocity perpendicular to the original motion can be found by integrating:

$$\begin{aligned}\Delta v_\perp &= \int_{-\infty}^{\infty} \frac{\mathrm{d}v_\perp}{\mathrm{d}t}\,\mathrm{d}t \;=\; \int_{-\infty}^{\infty} \frac{GMb}{(b^2 + v^2t^2)^{3/2}}\,\mathrm{d}t \\ &= \frac{GM}{vb}\int_{-\infty}^{\infty} \frac{\mathrm{d}x}{(1+x^2)^{3/2}} \;=\; \frac{2GM}{vb}\end{aligned}$$

In the third step we change variables $x = vt/b$ to make the integral dimensionless. The integral can then be evaluated by changing variables again to $x = \tan\theta$. Using $\Delta v_\perp$, we can write the **deflection angle** as

$$\hat{\alpha} \;\approx\; \tan\hat{\alpha} \;=\; \frac{\Delta v_\perp}{v} \;=\; \frac{2GM}{v^2 b}$$

where we use the small-angle approximation. Notice that the deflection angle is independent of the mass of the moving particle. It must apply to arbitrarily low

masses, and even to the limit $m \to 0$ as appropriate if we think of light as a photon. Therefore, we expect light to be bent by gravity.[2]

This analysis used Newtonian gravity. The analysis with general relativity (see Sect. 10.6.5) gives a bending angle that is the same for a massive particle, but a factor of 2 larger for a massless particle (like light). Therefore we can say:

$$\hat{\alpha} = \begin{cases} \dfrac{2GM}{v^2 b} & \text{massive, non-relativistic particle} \\ \dfrac{4GM}{c^2 b} & \text{massless particle} \end{cases} \tag{9.1}$$

It is possible to develop the theory of gravitational lensing in a relativistic framework (e.g., [1]), but for lensing by stars and galaxies it is adequate (and much simpler) to work in the Newtonian framework and insert the factor of 2 for light.[3]

Example: Deflection of Light by the Sun

The nearest object that creates measurable light bending is the Sun. Light from a distant star that passes just outside the surface of the Sun is deflected by the angle

$$\hat{\alpha}_\odot = \frac{4GM_\odot}{c^2 R_\odot} = \frac{4 \times (6.67 \times 10^{-11}\,\mathrm{m^3\,kg^{-1}\,s^{-2}}) \times (1.99 \times 10^{30}\,\mathrm{kg})}{(3.0 \times 10^8\,\mathrm{m\,s^{-1}})^2 \times (6.96 \times 10^8\,\mathrm{m})}$$

$$= 8.5 \times 10^{-6}\,\mathrm{rad} \times \frac{180\,\mathrm{deg}}{\pi\,\mathrm{rad}} \times \frac{3{,}600\,\mathrm{arcsec}}{1\,\mathrm{deg}} = 1.75\,\mathrm{arcsec}$$

Such starlight is normally swamped by light from the Sun, but it becomes visible during a solar eclipse. Frank Dyson and Arthur Eddington led expeditions to measure the positions of stars during an eclipse in 1919 [3]. They found that the positions were shifted (relative to the standard positions when the Sun is not present) by amounts that were consistent with Einstein's predictions (see Fig. 9.2). This measurement and a similar one by Campbell et al. during a 1922 eclipse [4] are considered to be among the classic tests of general relativity (see Sect. 10.4).

[2] You might wonder whether it makes sense to take the limit of the gravitational force as $m \to 0$, but in general relativity we learn that energy gravitates.

[3] Gravitational lensing by black holes does require a full relativistic treatment (see [2] for a review).

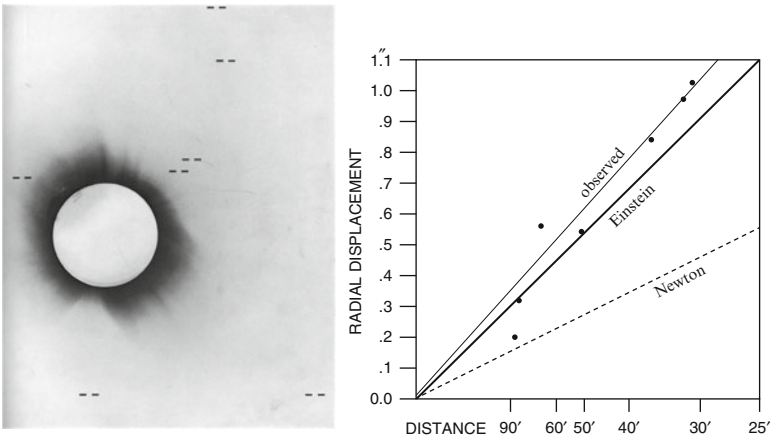

Fig. 9.2 The *left panel* shows a photographic negative from the solar eclipse of 1919. Although they are hard to see, star positions are marked. Comparing the positions in this picture with those measured when the Sun is not in the way yielded the deflections plotted in the *right panel*. (Note that the horizontal axis is inverted so stars closer to the Sun are plotted toward the right) (Credit: Dyson, Eddington and Davidson [3])

9.1.2 Lens Equation

If the impact parameter is small enough, light can go around both sides of the lensing mass and still reach Earth. In such **strong lensing**,[4] we see what appears to be the same light coming from two different directions, so we detect two images of the background source.

To quantify this effect, let D_l and D_s be the distances from the observer to the lens and source, respectively, and D_{ls} be the distance from the lens to the source. Using the small-angle approximation, we can define various distances perpendicular to the line of sight as shown on the left-hand side of Fig. 9.3. If we assume Euclidean geometry, we can write down the relation

$$D_s\beta = D_s\theta - D_{ls}\hat{\alpha}(\theta)$$

where we write $\hat{\alpha}(\theta)$ to remind ourselves that the deflection angle depends on the impact parameter, which in turn depends on θ. Rewriting this very slightly, we have

$$\beta = \theta - \alpha(\theta) \tag{9.2}$$

[4]"Strong" is a relative term; the bending angle is still in the small-angle regime.

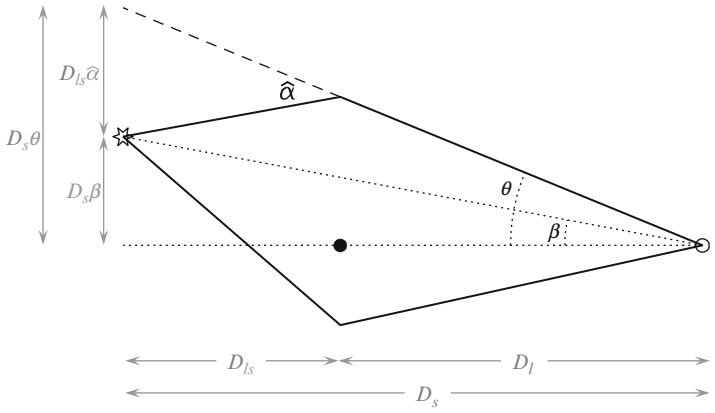

Fig. 9.3 The geometry of strong gravitational lensing. In this example, light can take two paths from the source (on the left) to the observer (on the right). The angle from the lens to the source is β, the angle from the lens to an observed image is θ, and the deflection angle is $\hat{\alpha}$. The distance from the observer to the lens is D_l, from the observer to the source is D_s, and from the lens to the source is D_{ls}. The lengths shown on the left assume the small-angle approximation

where we define the scaled deflection angle

$$\alpha(\theta) = \frac{D_{ls}}{D_s}\,\hat{\alpha}(\theta) \tag{9.3}$$

For lensing by galaxies, we cannot use Euclidean geometry to describe the expanding universe through which the light rays move. However, the bending happens only in close proximity to the galaxy, over a distance that is a small fraction of the total distance traveled. We can therefore view the trajectory as two "straight" lines (as generalized to an expanding universe) that are connected by a sharp bend. This is known as the **thin lens approximation**. It allows us to interpret Eq. (9.2) in a cosmological context provided that we take the distances D_l, D_s, and D_{ls} to be cosmological *angular diameter distances* (see Sect. 11.3.2 for details). The key point for now is that angular diameter distances do not add in a simple way, so $D_{ls} \neq D_s - D_l$ for cosmological lensing

In Fig. 9.3 all the light rays lie in a plane, which is true if the gravitational field is spherically symmetric and the force is purely radial. In general that may not be the case, but we can keep the same form of the lens equation if we interpret all the angles (β, θ, and α) as 2-dimensional vectors in the plane of the sky. In other words, $\boldsymbol{\theta}$ has two components (θ_1, θ_2) that measure angles in the east/west and north/south directions, respectively (and similar for $\boldsymbol{\beta}$ and $\boldsymbol{\alpha}$). This general form of the **lens equation** serves as the foundation for the theory of gravitational lensing. The vector form of α acts as a 2-d analog of the gravitational force, so in the same way that we define a potential via $\mathbf{F} = -\nabla U$ in 3-d, we can define a **lens potential** in 2-d via

$$\boldsymbol{\alpha} = \nabla\psi \tag{9.4}$$

(Note that we do not include a minus sign when defining the lens potential ψ, because we explicitly incorporate the sign into the lens equation.) Then we can write the lens equation as

$$\boldsymbol{\beta} = \boldsymbol{\theta} - \nabla\psi \tag{9.5}$$

9.1.3 Lensing by a Point Mass

To see some detail, let's consider lensing by a point mass. This is the application of the gravitational one-body problem to light bending. The scaled deflection angle is

$$\alpha \;=\; \frac{D_{ls}}{D_s}\,\frac{4GM}{c^2 b} \;=\; \frac{4GM}{c^2}\,\frac{D_{ls}}{D_l D_s}\,\frac{1}{\theta} \tag{9.6}$$

where we write the impact parameter as $b = D_l\theta$ in the small-angle approximation. It is convenient to define

$$\theta_E = \left(\frac{4GM}{c^2}\,\frac{D_{ls}}{D_l D_s}\right)^{1/2} \tag{9.7}$$

We will interpret this quantity momentarily. For now, it lets us write the lens equation as

$$\beta = \theta - \frac{\theta_E^2}{\theta}$$

Rearranging gives

$$\theta^2 - \beta\theta - \theta_E^2 = 0$$

which is a quadratic equation with two solutions,

$$\theta_\pm = \frac{1}{2}\left[\beta \pm \left(\beta^2 + 4\theta_E^2\right)^{1/2}\right] \tag{9.8}$$

Consider the case $\beta = 0$, so the solutions are $\theta_\pm = \pm\theta_E$. In this case the observer, lens, and source all lie on a line, so we can rotate the system around that line and have perfect symmetry. In other words, there are images that appear *all the way around the lens*, forming a perfect **Einstein ring** image. Since θ_E gives the angular size of the ring, we call it the **angular Einstein radius**.

In the general case $\beta \neq 0$, notice that

$$\theta_+ \geq \theta_E \quad \text{and} \quad -\theta_E \leq \theta_- < 0$$

The $+$ image is always outside the Einstein ring, while the $-$ image is always inside the Einstein ring and on the other side of the lens (as indicated by the minus sign). Now consider:

$$\begin{aligned}\theta_+ \, \theta_- &= \frac{1}{2}\left[\beta + (\beta^2 + 4\theta_E^2)^{1/2}\right] \times \frac{1}{2}\left[\beta - (\beta^2 + 4\theta_E^2)^{1/2}\right] \\ &= \frac{1}{4}\left[\beta^2 - (\beta^2 + 4\theta_E^2)\right] \\ &= -\theta_E^2\end{aligned}$$

Substituting for θ_E from Eq. (9.7), we can solve for mass:

$$M = \frac{c^2}{4G} \, \frac{D_l \, D_s}{D_{ls}} \, |\theta_+ \, \theta_-| \tag{9.9}$$

If we observe two lensed images, and we know the distances involved, we can compute the mass of the lens. This is the motion $\rightarrow$ mass principle for gravitational lensing. What is different now is that we are using the motion of *light* to measure mass.

In Fig. 9.4, the left and middle columns show examples of lensing by a point mass. Each source produces two images, one on the same side of the lens as the source and outside θ_E, the other on the opposite side and inside θ_E. The exception is a source directly behind the lens, which produces a complete Einstein ring. The right column shows an example in which the gravitational field is not spherically symmetric, which we will examine below. In that case lensing can produce four images for certain source positions. Figure 9.5 shows an example of an observed 4-image lens system.

9.1.4 Distortion and Magnification

In Fig. 9.4 we see that lensed images can be stretched, and in Fig. 9.5 we see that images of a single source can have different brightnesses. Thus, the observable effects of lensing include distortion and magnification. To illustrate how these occur, Fig. 9.6 shows the images of a straight arrow source behind a point mass lens. The outer image is created when each piece of the source arrow is pushed radially outward until it lies beyond the Einstein radius. The image subtends the same

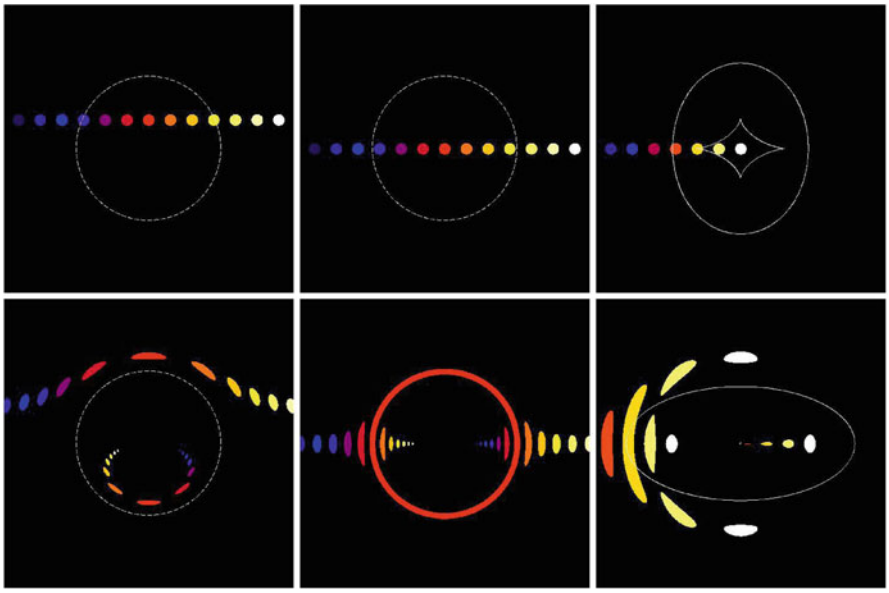

Fig. 9.4 Examples of strong gravitational lensing. The *top row* shows arrays of sources, while the *bottom row* shows the resulting lensed images (colored the same as the sources). In the *left* and *middle columns*, the lens is a point mass; the *dashed circle* indicates the Einstein radius. The difference is whether the sources are offset from or aligned with the middle of the lens. A source directly behind a circular lens produces an Einstein ring (*bottom middle*). In the *right column*, the lens is an ellipsoidal galaxy model; the *dashed curves* indicate the "critical curves" (in the image plane) and "caustics" (in the source plane). A source within the inner caustic produces four images

azimuthal angle as the source,[5] but since it lies at a larger radius it winds up being longer. The inner image is created when each piece of the source is pushed radially "through" the center of the lens. Again the image subtends the same azimuthal angle as the source, but it can lie close to the center and thus be short, or it can lie near (but inside) the Einstein radius and thus be relatively long (as in the example). Notice that the outer image gets distorted but retains the same orientation as the source. By contrast, the inner image gets flipped upside down while keeping the same left/right orientation as the source. There is no way to obtain this image by distorting and rotating the source, so we say the **parity** (or handedness) of the inner image has been reversed.

[5]Having the image subtend *exactly* the same azimuthal angle as the source requires a radial deflection and thus is limited to circular lenses. The concept of tangential stretching is general, though.

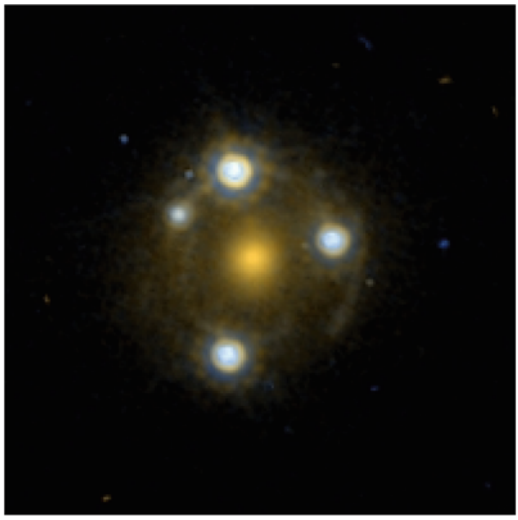

Fig. 9.5 Hubble Space Telescope image of the four-image gravitational lens SDSS J0924−0219. The *red-orange* object in the middle is the lens galaxy, while the four *blue-white* objects are lensed images of a background quasar (Credit: Keeton et al. [5]. Reproduced by permission of the AAS)

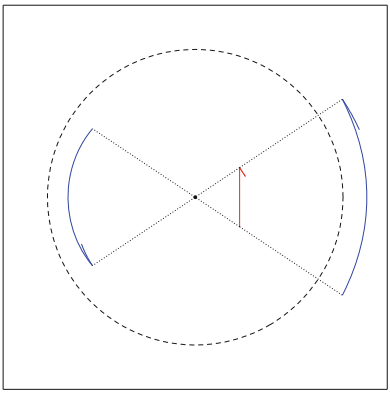

Fig. 9.6 Example of lensing distortion and magnification. The straight *red arrow* shows the source; the *curved blue arrows* show the two lensed images. The outer image has the same parity as the source, but the inner image has the opposite parity. The *dashed circle* indicates the Einstein radius. The *dotted lines* show that, for a spherical lens, each part of the source yields two images on radial lines

To quantify these effects, consider a small displacement $\Delta\boldsymbol{\beta}$ in the source plane. It will map to a small displacement in the image plane given by

$$\Delta\boldsymbol{\theta} = \frac{\partial\boldsymbol{\theta}}{\partial\boldsymbol{\beta}}\,\Delta\boldsymbol{\beta} \tag{9.10}$$

Since $\Delta\boldsymbol{\theta}$ and $\Delta\boldsymbol{\beta}$ are 2-d vectors, the quantity $\mathsf{A} \equiv \partial\boldsymbol{\theta}/\partial\boldsymbol{\beta}$ is a 2×2 tensor. It specifies how the shape of a (small) source is changed by lensing, so we call it the **amplification tensor**. It is actually easier to compute the inverse using the lens equation:

$$\mathsf{A}^{-1} = \frac{\partial\boldsymbol{\beta}}{\partial\boldsymbol{\theta}} = \begin{bmatrix} 1 - \frac{\partial\alpha_1}{\partial\theta_1} & -\frac{\partial\alpha_1}{\partial\theta_2} \\ -\frac{\partial\alpha_2}{\partial\theta_1} & 1 - \frac{\partial\alpha_2}{\partial\theta_2} \end{bmatrix} = \begin{bmatrix} 1 - \frac{\partial^2\psi}{\partial\theta_1^2} & -\frac{\partial^2\psi}{\partial\theta_1\partial\theta_2} \\ -\frac{\partial^2\psi}{\partial\theta_1\partial\theta_2} & 1 - \frac{\partial^2\psi}{\partial\theta_2^2} \end{bmatrix} \tag{9.11}$$

Here subscripts indicate components of a 2-d vector on the sky (see Sect. 9.1.2). In the last step we use Eq. (9.4) and see explicitly that A is symmetric.

To characterize the distortion and magnification of a small source, we introduce three quantities $(\kappa, \gamma_+, \gamma_\times)$ defined by

$$\mathsf{A}^{-1} = \begin{bmatrix} 1 - \kappa - \gamma_+ & -\gamma_\times \\ -\gamma_\times & 1 - \kappa + \gamma_+ \end{bmatrix} \tag{9.12}$$

Comparing this with Eq. (9.11) lets us write

$$\kappa = \frac{1}{2}\left(\frac{\partial^2\psi}{\partial\theta_1^2} + \frac{\partial^2\psi}{\partial\theta_2^2}\right) \tag{9.13a}$$

$$\gamma_+ = \frac{1}{2}\left(\frac{\partial^2\psi}{\partial\theta_1^2} - \frac{\partial^2\psi}{\partial\theta_2^2}\right) \tag{9.13b}$$

$$\gamma_\times = \frac{\partial^2\psi}{\partial\theta_1\,\partial\theta_2} \tag{9.13c}$$

In Problem 9.1 you can learn that $\kappa > 0$ makes a source look bigger; it is related to focusing of light, so it is known as **convergence**. By contrast, γ_+ and $\gamma_\times$ cause a source to look distorted, so they are known as **shear**. Strictly speaking, the convergence and shear describe what happens to a source that is small enough for $(\kappa, \gamma_+, \gamma_\times)$ to be constant across the source, but they offer an intuitive sense of what happens to larger sources as well.

Lensing conserves surface brightness (it merely redirects photons, without creating or destroying any), so if a small source has surface brightness I and area $\mathrm{d}A_{\rm src}$ and it leads to an image with area $\mathrm{d}A_{\rm img}$, then the ratio of fluxes is

$$\frac{f_{\rm img}}{f_{\rm src}} = \frac{I\,\mathrm{d}A_{\rm img}}{I\,\mathrm{d}A_{\rm src}} = \frac{\mathrm{d}A_{\rm img}}{\mathrm{d}A_{\rm src}} = |\det\mathsf{A}|$$

Thus we define

$$\mu \equiv \det\mathsf{A} \tag{9.14}$$

to be the **lensing magnification** such that the ratio of fluxes is $f_{\rm img}/f_{\rm src} = |\mu|$. We could make the absolute value part of the definition of μ, but it is convenient to let μ be a signed quantity because the sign reveals the parity of the image. If the source is large enough that we can resolve the images, then we observe the shapes directly and so we work with A itself. By contrast, if the source is small and we cannot resolve the images, then we only measure fluxes and so we work with μ. Using Eq. (9.12) we can write the magnification in terms of the convergence and shear:

$$\mu = \left[(1-\kappa)^2 - \gamma_+^2 - \gamma_\times^2\right]^{-1} \tag{9.15}$$

Circular Symmetry

If the lens has circular symmetry, the potential and deflection are functions of $\theta = (\theta_1^2 + \theta_2^2)^{1/2}$. Then working out the derivatives and using some trigonometry (see Problem 9.2) gives

$$\mu = \left(1 - \frac{\alpha}{\theta}\right)^{-1} \left(1 - \frac{{\rm d}\alpha}{{\rm d}\theta}\right)^{-1} \tag{9.16}$$

Recall that the Einstein radius satisfies $\theta_E - \alpha(\theta_E) = 0$, so at the Einstein radius the first factor vanishes and hence the magnification diverges. For an image near but not precisely at θ_E, the magnification will be finite but it can be large. This is reflected in the size and shape of images near the Einstein radius in Fig. 9.4. In multiply-imaged quasars it is not uncommon for the brightest images to have magnifications of 10 or 20, and in some cases of microlensing (Sect. 9.2) magnifications of hundreds or even thousands have been recorded [6, 7].

Point Mass

For a point mass, using $\alpha = \theta_E^2/\theta$ in Eq. (9.16) leads to a magnification

$$\mu = \left(1 - \frac{\theta_E^2}{\theta^2}\right)^{-1} \left(1 + \frac{\theta_E^2}{\theta^2}\right)^{-1} = \frac{\theta^4}{\theta^4 - \theta_E^4}$$

Recall that the $+$ image has $\theta_+ \geq \theta_E$, so the denominator is positive, and indeed the entire quantity is larger than 1; this image is always brighter than the source. By contrast, the $-$ image has $|\theta_-| \leq \theta_E$, so the denominator and hence the magnification is negative. The sign reflects the parity reversal. There is no lower bound on $|\mu|$ for the $-$ image, so this image can be bright or faint. For both images, when θ approaches θ_E the magnification gets arbitrarily large.

9.1.5 *Time Delay*

Looking back at Fig. 9.3, notice that each light ray is longer than it would have been if it went straight from the source to the observer. Also, each light ray experiences a relativistic phenomenon called gravitational time dilation (see Sect. 10.2.3). The two effects cause the light to take longer to reach us along the lensed path than it would have along the direct route (without lensing). The excess light travel time, which is called the lens **time delay**, is

$$\tau = \frac{1+z_l}{c}\frac{D_l D_s}{D_{ls}}\left[\frac{1}{2}|\boldsymbol{\theta}-\boldsymbol{\beta}|^2 - \psi(\boldsymbol{\theta})\right] \tag{9.17}$$

where z_l is the cosmological redshift of the lens (see Sect. 11.3.1). The first term in square brackets quantifies the extra distance the light has to travel, while the second term encodes gravitational time dilation.

Usually we cannot measure the time delay itself, because we cannot know how long it would have taken the light to reach us without lensing, but we can measure the *differential* time delay between two images. Time delays are thus another observable aspect of lensing, although we will not say much more about them here. One conceptual point is that time delays provide a new way to think about where the lens equation comes from. By Fermat's principle, light will "choose" trajectories that correspond to stationary points of the travel time function.[6] The condition $\nabla\tau = 0$ immediately yields $\boldsymbol{\theta} - \boldsymbol{\beta} - \nabla\psi = 0$, which is the lens equation (9.5). In other words, images form at stationary points of the time delay surface.

9.2 Microlensing

In the remainder of this chapter we examine several ways in which gravitational lensing can be used to investigate matter that is difficult or impossible to observe directly. Let's begin in our own Milky Way galaxy. Once galaxy rotation curves gave evidence for dark matter, people begin to wonder what the extra mass is made of. Two competing hypotheses emerged[7]:

- **MACHOs**, or Massive Astrophysical Compact Halo Objects. According to this hypothesis, dark matter is composed of astrophysical objects that are faint but otherwise familiar. Possibilities include: brown dwarf stars, which are balls of

[6] You may be familiar with the principle of least time, but local minima are not the only stationary points. As a function of two dimensions, τ can also have local maxima and saddle points.

[7] Don't blame me—I didn't invent the names! For the record, "WIMP" was introduced first, and "MACHO" was chosen deliberately (see [8]).

gas that are too small to support nuclear fusion, so they do not shine (see Problem 16.5); white dwarf stars, which are dim stellar corpses (see Sect. 17.2); planets; or black holes.
- **WIMPs**, or Weakly Interacting Massive Particles. According to this hypothesis, dark matter is a fundamental particle that is unfamiliar to us. There are many hypothetical particles that could have the right properties to act as dark matter, including neutralinos, axions, gravitinos, and much more (see [9]).

If dark matter is made of MACHOs, the Milky Way should be rife with objects the mass of planets or stars that can cause a form of lensing known as microlensing. If dark matter is instead made of WIMPs, it should be spread more diffusely, which would limit microlensing to events produced by stars. Measuring the rate of lensing in our own galaxy can therefore help us distinguish between MACHO and WIMPy dark matter.

9.2.1 Theory

Consider using a star in the Milky Way as the source of light, and either another star or a MACHO in the foreground as the lens. In a typical scenario the source is a star in the bulge of our galaxy, which is about 8 kpc away, and the lens is a star roughly halfway in between. The Einstein radius for a solar mass star is then

$$\begin{aligned}\theta_E &= \left[\frac{4\times(6.67\times10^{-11}\,\mathrm{m^3\,kg^{-1}\,s^{-2}})\times(1.99\times10^{30}\,\mathrm{kg})}{(3.0\times10^{8}\,\mathrm{m\,s^{-1}})^2}\times\frac{1}{8\times3.09\times10^{19}\,\mathrm{m}}\right]^{1/2}\\ &= 4.9\times10^{-9}\,\mathrm{rad}\times\frac{180\,\mathrm{deg}}{\pi\,\mathrm{rad}}\times\frac{3600\,\mathrm{arcsec}}{1\,\mathrm{deg}}\\ &= 0.001\,\mathrm{arcsec}\end{aligned}$$

Since the Einstein radius is so small, the images are too close together to be resolved (even with the Hubble Space Telescope). As the source and lens move through the galaxy, though, the positions and brightnesses of the images change with time. We can detect microlensing through variations in the apparent brightness of the source star.

Problem 9.4 you can practice solving the lens equation to predict the changes in brightness as the source moves relative to the lens. For now let us focus on the time scale for variability. The natural scale is the time it takes for the source and lens to move (relative to the each other) by the diameter of the Einstein ring. Since θ_E is the angular Einstein radius, the corresponding length is $D_l\theta_E$. The speed that matters is the relative velocity of the lens and source perpendicular to the line of sight, which we write as $v_\perp$. The typical **Einstein crossing time** is therefore

$$t_E = \frac{2D_l\theta_E}{v_\perp} = \frac{2}{v_\perp}\left(\frac{4GM}{c^2}\,\frac{D_l D_{ls}}{D_s}\right)^{1/2} \tag{9.18}$$

For the typical values quoted above and $v_\perp = 200\,\mathrm{km\,s^{-1}}$, the time scale is $t_E = 70$ days. This is quite convenient: short enough that impatient astronomers do not have to wait too long, but long enough that they can make many measurements during the course of an event even if some nights are lost to bad weather.

9.2.2 *Observations*

The biggest observational challenge is the low probability for any given star to be microlensed (which you can estimate in Problem 9.5). If you watch enough stars over a long enough period of time, however, you are bound to see some events. The prospect of testing the MACHO hypothesis was tantalizing enough to lead several groups to make a concerted effort to look for microlensing. Three of the main teams were the MACHO Project, the Optical Gravitational Lensing Experiment (OGLE), and Expérience pour la Recherche d'Objets Sombres (EROS). To give a sense of scale: the MACHO Project monitored about 17 million stars toward the center of the Milky Way for 3 years and observed 99 events, and also monitored almost 12 million stars in the Large Magellanic Cloud (LMC, a small galaxy orbiting the Milky Way) for almost 6 years and observed 13–17 events (depending on the selection criteria) [10,11]. Looking toward the Galactic Center raised the odds that the team would see at least a few events and thus validate their observational methods, while looking toward the LMC let them look through the Milky Way's halo to search for MACHO dark matter.

Two sample microlensing events are shown in Fig. 9.7. Each star was observed in both red and blue light to distinguish lensing from other effects. Light bending is independent of wavelength, so a microlensing event ought to look the same in both red and blue light.[8] Most of the time the light curve is constant (revealing the star's natural flux). But during a period of a few months the star brightens, reaches a peak, and then fades back to its original flux. The measured data points nicely follow the predicted microlensing light curve. For each event, we can measure the peak magnification, which depends on how close the source star came to the lens, and the duration of the event, which depends on a combination of the mass of the lens, the distances, and the relative velocity (see Eq. 9.18). While this information does not uniquely determine the mass of the lens star, it does at least confirm that we saw microlensing.

As we said, the idea is to see whether the number of microlensing events is comparable to or higher than the number expected from known populations of stars in the Milky Way. The analysis is necessarily detailed; suffice it to say that the

[8] By contrast, variable stars tend to change color as they change brightness.

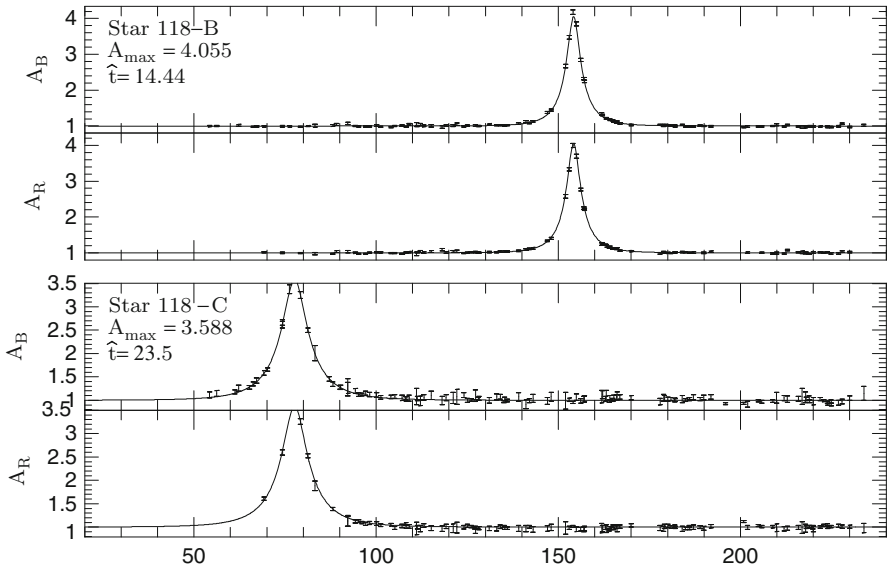

Fig. 9.7 Microlensing light curves for two stars from the MACHO project. Each pair of panels shows the same star in *red* and *blue light*. The horizontal time axis is measured in days. The points with errorbars show the measured brightness, while the curves show microlensing models (Credit: Alcock et al. [12]. Reproduced by permission of the AAS)

microlensing event rate is much lower than expected if all the dark matter were MACHOs [11]. There may be some but not very many MACHOs in the Milky Way. Dark matter, it seems, is mostly WIMPy.

9.2.3 Binary Lenses

Observed light curves do not always match standard predictions as well as the ones in Fig. 9.7. Many of them have features that arise when the lens star has a companion: either another star or a planet. The gravitational field for a binary lens is sufficiently complicated that we cannot predict the light curve analytically. Nevertheless, we can understand some of the distinctive phenomena that occur in binary lensing.

Consider the case of two equal mass stars, and a source star directly behind the center of mass. The resulting image configuration is shown in Fig. 9.8. Image #1 appears right in the middle because the gravity from the star on the right cancels the gravity from the star on the left. Image #2 appears where it does because both stars pull the light to the right; and vice versa for image #3. For image #4, both stars pull down, while the leftward and rightward forces cancel; and vice versa for image #5.

The key concept is that there can be *five* images. This is true not only for a source right between the stars, but also for some other positions. As shown in Fig. 9.9, there

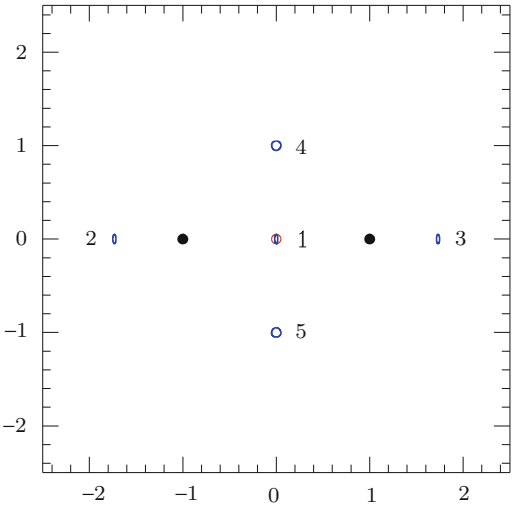

Fig. 9.8 Images produced when a source is directly behind the center of a lens consisting of two equal-mass stars

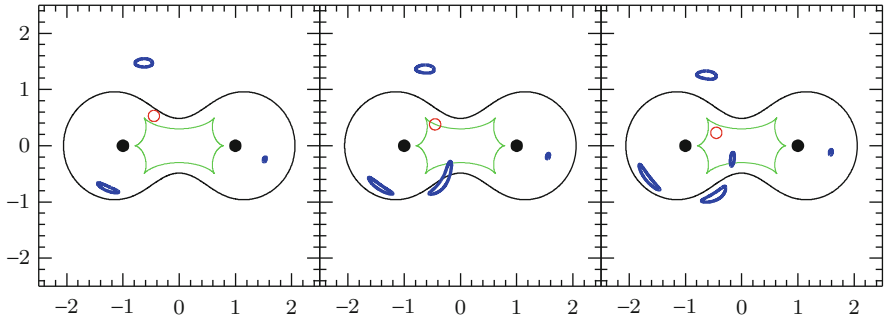

Fig. 9.9 Illustration of binary lensing. In each panel, the *green curve* shows the caustic, the *black curve* shows the corresponding critical curve, the *red circle* shows the source, and the *blue curves* show the lensed images

is a region in the source plane that leads to five images, and another region that leads to three. The boundary between them is called a **caustic curve** in the source plane. Caustics map to **critical curves** in the image plane, which are like the Einstein ring but generalized to scenarios without circular symmetry. Caustics mark where the number of images changes. A source just inside a caustic produces two images near a critical curve that are highly magnified and distorted. (If the source straddles the caustic, the two images merge into one that crosses the critical curve.) Consequently, the lensing magnification can change dramatically from one side of the caustic to the other.

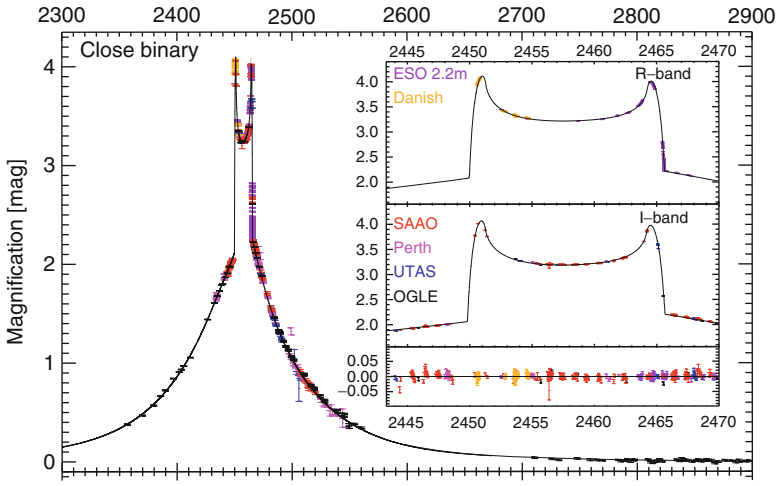

Fig. 9.10 Light curve for a binary microlensing event. The vertical axis is labeled magnification but is actually $2.5 \log |\mu|$, so the highest points correspond to magnifications of around 40. The *colored points* show data from different telescopes. The curve shows a binary lens model. In the inset, the two *upper panels* show results for different filters, while the *bottom panel* shows the residuals between the data and model (Credit: Kubas et al. [13]. Reproduced with permission © ESO)

We can see this as a sharp change in the magnification when a source moves across a caustic during a microlensing event, as shown in Fig. 9.10. The main plot shows the full light curve. The inset shows a close-up of the caustic crossing event; the colored points show the data, while the black curve shows a theoretical prediction. Remarkably, the light curve depends not only on the properties of the lens (the masses and positions of the two stars), but also on the structure of the source. At any given time the part of the source that is right on the caustic is dramatically magnified. As the source moves across the caustic, different portions of its surface are magnified in turn, and the light curve essentially maps the surface of the star (in the direction of motion, at least). In this way microlensing effectively boosts the resolving power of our telescopes to help us study structures that would otherwise be too small to see.

9.2.4 Planets

If we reduce the companion mass to the scale a planet, the caustics shrink to the point that the gravity from the planet just produces a "blip" on the light curve. The time scale for the planetary feature, compared to the full stellar event, is

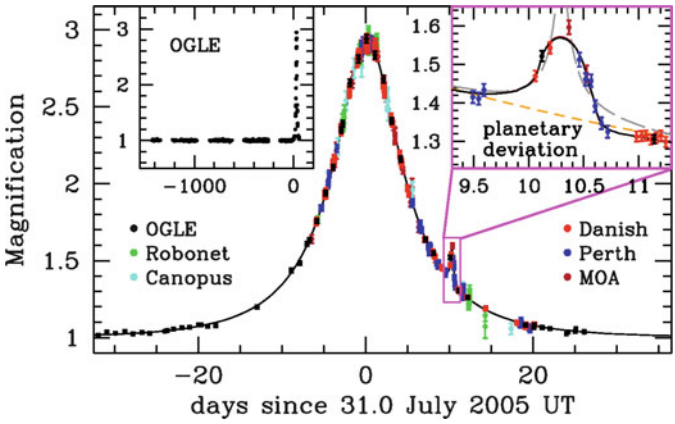

Fig. 9.11 Microlensing light curve revealing a planet estimated to be about 5.5 Earth masses (Reprinted by permission from Macmillan Publishers Ltd: Beaulieu et al. [15], © 2006)

$$\frac{t_{\text{planet}}}{t_{\text{star}}} = \frac{2D_l\theta_{\text{planet}}/v_\perp}{2D_l\theta_{\text{star}}/v_\perp} = \left(\frac{M_{\text{planet}}}{M_{\text{star}}}\right)^{1/2}$$

For the Sun and Jupiter, the mass ratio translates into a duration ratio of $t_{\text{planet}}/t_{\text{star}} = 0.031$. With the typical numbers from Sect. 9.2.1, the planetary event would last about $t_{\text{planet}} \sim 2$ days. For the Sun and Earth, the numbers are $t_{\text{planet}}/t_{\text{star}} = 0.0017$ and $t_{\text{planet}} \sim 3\,\text{h}$.

Planetary microlensing events are short enough that they require continuous monitoring by telescopes around the world. To do this efficiently, microlensing observers developed a strategy in which the main teams would observe their large samples of stars once a week or so. When they spotted a star in the early stages of a microlensing event, they would broadcast an alert so that other teams could begin using other telescopes to monitor the event very closely. This strategy has paid off with the discovery of more than a dozen microlensing planets so far [14]. Figure 9.11 shows a planetary event discovered in August 2005 after an alert from the OGLE team.

Beyond merely detecting a planet, what did they learn from this event? The most well-constrained quantity is the mass ratio between the planet and star, which basically comes from the ratio of time scales [15]:

$$\frac{M_{\text{planet}}}{M_{\text{star}}} = (7.6 \pm 0.7) \times 10^{-5}$$

To estimate the actual masses of the star and planet, the team had to make a detailed model of the population of stars in the galaxy and figure out which ones are most likely to produce an event like the one seen. This yielded

$$M_{\text{star}} = 0.22^{+0.21}_{-0.11}\, M_\odot \quad \text{and} \quad M_{\text{planet}} = 5.5^{+5.5}_{-2.7}\, M_\oplus$$

The uncertainties are significant: the planet could be only a few times more massive than Earth, or more than 10 times more massive. This is the best that can be done without direct knowledge of the distance to the lens or the relative velocity between the lens and source. Still, it allows the important conclusion that this planet is in the same league as Neptune.

While microlensing has revealed fewer exoplanets than the Doppler and transit techniques (see Sect. 4.3), it serves as a valuable complement. Microlensing involves completely different physical processes and observational methods, so it provides independent confirmation that other stars have planets. Also, microlensing is more sensitive to small planets far from their stars. Finally, microlensing is better able to examine stars that are far from Earth. The main drawback is that we only see a microlensing event once, when the star and planet cross in front of a background source; after the event concludes, it cannot be repeated. Therefore microlensing will probably contribute more to a statistical census of planets rather than to detailed knowledge of individual systems. Nevertheless, microlensing is expected to play an increasingly important role in planet searches in the coming decade.

9.3 Strong Lensing

With stars and planets it is reasonable to use the point mass approximation, but when we turn to galaxies and clusters of galaxies we must consider extended mass distributions.

9.3.1 Extended Mass Distribution

We can still work in the thin lens approximation, so what matters is the projected surface mass density of the galaxy, Σ. A small patch of the lens at position $\boldsymbol{\theta}'$ has mass $\Sigma(\boldsymbol{\theta}')\,\mathrm{d}\boldsymbol{\theta}'$, so the amount of bending it creates at $\boldsymbol{\theta}$ is

$$\mathrm{d}\boldsymbol{\alpha}(\boldsymbol{\theta}) = \frac{4G}{c^2}\frac{D_{ls}}{D_l D_s}\Sigma(\boldsymbol{\theta}')\frac{\boldsymbol{\theta}-\boldsymbol{\theta}'}{|\boldsymbol{\theta}-\boldsymbol{\theta}'|^2}\,\mathrm{d}\boldsymbol{\theta}'$$

(This is the 2-d vector form of Eq. 9.6.) We can therefore write the total scaled deflection as

$$\boldsymbol{\alpha}(\boldsymbol{\theta}) = \frac{1}{\pi}\int \frac{\Sigma(\boldsymbol{\theta}')}{\Sigma_{\mathrm{crit}}}\frac{\boldsymbol{\theta}-\boldsymbol{\theta}'}{|\boldsymbol{\theta}-\boldsymbol{\theta}'|^2}\,\mathrm{d}\boldsymbol{\theta}' \tag{9.19}$$

where we have collected multiplicative factors and defined

$$\Sigma_{\mathrm{crit}} = \frac{c^2}{4\pi G}\frac{D_l D_s}{D_{ls}} \tag{9.20}$$

We call this the **critical surface density** for lensing, for reasons that will become clear shortly. If we take the divergence $\nabla \cdot \boldsymbol{\alpha}$ and recall that the deflection is related to the lens potential by $\boldsymbol{\alpha} = \nabla\psi$, we obtain

$$\nabla^2\psi = 2\frac{\Sigma}{\Sigma_{\rm crit}} \tag{9.21}$$

This has the form of the Poisson equation for the gravitational potential, but in two dimensions. It provides the general framework for lensing by arbitrary 2-d mass distributions. By comparing Eqs. (9.13a) and (9.21), we see that the convergence is the surface mass density scaled by the critical density:

$$\kappa = \frac{\Sigma}{\Sigma_{\rm crit}} \tag{9.22}$$

9.3.2 Circular Mass Distribution

For a mass distribution with circular symmetry, we can evaluate Eq. (9.19) using an analog of Newton's theorem about gravity from a spherical mass distribution. Recall from Sect. 2.3 that Newton found $F(r) \propto M(r)/r^2$ where $M(r)$ is the mass enclosed within r. The radial dependence is $1/r^2$ because a certain "amount of gravity" is spread over a spherical shell whose area scales as r^2. By analogy, in 2-d the dependence should be $1/R$, or in terms of the angular impact parameter $1/\theta$. Indeed, the scaled deflection from a circular mass distribution is

$$\alpha(\theta) = \frac{4G}{c^2}\frac{D_{ls}}{D_l D_s}\frac{M(\theta)}{\theta} \tag{9.23}$$

Recalling that the Einstein radius is defined by $\alpha(\theta_E) = \theta_E$, we can write

$$M(\theta_E) = \frac{c^2}{4G}\frac{D_l D_s}{D_{ls}}\theta_E^2 \tag{9.24}$$

If we see an Einstein ring, we can infer the mass enclosed by the ring even if we do not know the density profile. If we do not see a complete ring, the principle still holds that the quantity we measure best is the mass within θ_E. This is how we can use gravitational lensing as a tool to weigh distant galaxies and clusters of galaxies.

Consider the average surface mass density enclosed by the Einstein ring (in angular units, e.g., solar masses per square arcsecond):

$$\langle\Sigma\rangle = \frac{M(\theta_E)}{\pi\theta_E^2} = \frac{c^2}{4\pi G}\frac{D_l D_s}{D_{ls}} = \Sigma_{\rm crit}$$

All Einstein rings enclose an average density that is given by $\Sigma_{\rm crit}$ from Eq. (9.20). Put another way, an object must have $\Sigma \geq \Sigma_{\rm crit}$ in order to have an Einstein ring at all. This is the sense in which $\Sigma_{\rm crit}$ is the critical density for lensing.

9.3.3 Singular Isothermal Sphere

A specific example of an extended, circular mass distribution is the Singular Isothermal Sphere (SIS), which we first encountered when studying spiral galaxies (Sect. 7.3.2). With spiral galaxy rotation curves we used the (softened) isothermal model as one part of a multi-component model that also included contributions from a disk and bulge. With lensing we can often get away with even simpler models, because we mostly deal with elliptical galaxies where the stellar distribution is roundish like the dark matter halo, we focus on the *total* mass distribution (light bending depends only on the total amount of matter, not whether it is luminous or dark), and we only need to know the *projected* surface mass density. For all of these reasons, the singular isothermal sphere (and its generalization to an ellipsoid; Sect. 9.3.4) turns out to be a valuable model for lensing. An isothermal sphere with circular velocity v_c has a 3-d density profile[9]

$$\rho = \frac{v_c^2}{4\pi G r^2} = \frac{v_c^2}{4\pi G(R^2+z^2)}$$

where r is the spherical radius and (R,z) are cylindrical coordinates. The mass enclosed by the angle θ is obtained by integrating over R out to $D_l\theta$ and integrating over all z:

$$M(\theta) = \int_{-\infty}^{\infty} {\rm d}z \int_0^{D_l\theta} {\rm d}R\, 2\pi R\, \frac{v_c^2}{4\pi G(R^2+z^2)} = \frac{\pi}{2}\frac{v_c^2 D_l \theta}{G}$$

The scaled deflection angle is then

$$\alpha = \frac{4G}{c^2}\frac{D_{ls}}{D_l D_s}\frac{\pi}{2}\frac{v_c^2 D_l}{G} = 2\pi\left(\frac{v}{c}\right)^2 \frac{D_{ls}}{D_s}$$

The deflection is *independent of position*. The constant deflection angle is directly related to the constant circular velocity that we encountered when studying spiral galaxy dynamics (see Sect. 7.3). Clearly the Einstein radius is $\theta_E = \alpha$. To be more precise, we should take into account the direction of the deflection:

$$\alpha(\theta) = \begin{cases} +\theta_E & \theta > 0 \\ -\theta_E & \theta < 0 \end{cases}$$

[9] The SIS model can also be expressed in terms of the velocity dispersion, which is $\sigma = v_c/\sqrt{2}$.

We can then write the lens equation as:

$$\theta > 0: \quad \beta = \theta - \theta_E \tag{9.25a}$$

$$\theta < 0: \quad \beta = \theta + \theta_E \tag{9.25b}$$

Without loss of generality we can take $\beta \geq 0$. Then we can solve Eq. (9.25a) to find one of the images:

$$\theta_+ = \beta + \theta_E$$

We can also solve Eq. (9.25b):

$$\theta_- = \beta - \theta_E \qquad \text{only if } \beta \leq \theta_E$$

(If $\beta > \theta_E$ this equation would imply $\theta_- > 0$, which would violate the condition in Eq. 9.25b.) A singular isothermal sphere, in other words, can produce three types of configurations:

$$\begin{aligned} \beta = 0: &\ \text{Einstein ring at } \theta_E \\ 0 < \beta \leq \theta_E: &\ \text{two images at } \theta_\pm = \beta \pm \theta_E \\ \beta > \theta_E: &\ \text{one image at } \theta_+ = \beta + \theta_E \end{aligned}$$

Whereas a point mass lens always produces two images, an SIS lens creates two images only for sources in a finite region behind the lens.

9.3.4 Singular Isothermal Ellipsoid

Few galaxies are perfectly spherical, and new lensing phenomena appear when spherical symmetry is broken (see Figs. 9.4 and 9.9), so it worthwhile to consider the case of ellipsoidal symmetry. With circular symmetry the surface mass density Σ is a function of the polar radius $\theta = (\theta_1^2 + \theta_2^2)^{1/2}$. To make the symmetry elliptical instead, we can write Σ in terms of the ellipse coordinate $\xi = (\theta_1^2 + \theta_2^2/q^2)^{1/2}$ where $0 < q \leq 1$ is a dimensionless parameter that measures the ratio of the short and long axes: for $q = 1$ the model is again spherical, but for $q < 1$ it is flattened.

With elliptical symmetry it can be difficult to evaluate the integral in Eq. (9.19). The singular isothermal ellipsoid (SIE) is one case that can be treated analytically, leading to the lens equation [16]

$$\beta_1 = \theta_1 - \frac{\theta_E q}{(1-q^2)^{1/2}} \tan^{-1}\left[\frac{(1-q^2)^{1/2}\theta_1}{(q^2\theta_1^2 + \theta_2^2)^{1/2}}\right] \tag{9.26a}$$

$$\beta_2 = \theta_2 - \frac{\theta_E q}{(1-q^2)^{1/2}} \tanh^{-1}\left[\frac{(1-q^2)^{1/2}\theta_2}{(q^2\theta_1^2+\theta_2^2)^{1/2}}\right] \tag{9.26b}$$

Consider a source at the origin ($\beta_1 = \beta_2 = 0$). If we put $\theta_1 = 0$ then Eq. (9.26a) is trivially satisfied and Eq. (9.26b) becomes

$$0 = \theta_2 - \frac{\theta_E q}{(1-q^2)^{1/2}} \tanh^{-1}\left[(1-q^2)^{1/2}\,\mathrm{sgn}(\theta_2)\right]$$

which can be solved by

$$\theta_2 = \pm\frac{\theta_E q}{(1-q^2)^{1/2}} \tanh^{-1}(1-q^2)^{1/2}$$

Alternatively, if we go back to the equations and put $\theta_2 = 0$, then Eq. (9.26b) is trivially satisfied and Eq. (9.26a) becomes

$$0 = \theta_1 - \frac{\theta_E q}{(1-q^2)^{1/2}} \tan^{-1}\left[\frac{(1-q^2)^{1/2}}{q}\,\mathrm{sgn}(\theta_1)\right]$$

which can be solved by

$$\theta_1 = \pm\frac{\theta_E q}{(1-q^2)^{1/2}} \tan^{-1}\frac{(1-q^2)^{1/2}}{q}$$

While these expressions are admittedly non-intuitive, the main conceptual point is straightforward: a source at the origin yields four images, with two on the horizontal axis and two on the vertical axis. Figure 9.4 shows that other source positions can also yield four images.

9.3.5 Spherical Galaxy with External Shear

We can capture a lot of the same phenomenology using simpler algebra if we revert to a spherical model but account for the gravitational influence of other galaxies that happen to lie near the main lens galaxy. If the neighboring galaxies lie more than a few Einstein radii away, their effects can be characterized using a tensor of the form given in Eq. (9.12) where κ, γ_+, and $\gamma_\times$ are constant across the main lens galaxy.[10] If we choose coordinates such that $\gamma_\times = 0$, the lens equation has the form

[10]The shear is basically a tidal effect analogous to what we studied in Chap. 5.

$$\beta_1 = \theta_1 - \frac{\theta_E\,\theta_1}{(\theta_1^2+\theta_2^2)^{1/2}} - (\kappa+\gamma)\theta_1 \tag{9.27a}$$

$$\beta_2 = \theta_2 - \frac{\theta_E\,\theta_2}{(\theta_1^2+\theta_2^2)^{1/2}} - (\kappa-\gamma)\theta_2 \tag{9.27b}$$

We can now examine how the "external" shear[11] influences the number of images. Typical values of external shear are $\gamma \sim 0.01$–0.1. In what follows we set $\kappa = 0$ for simplicity, because it does not actually affect the image multiplicity.

For a source at the origin, an analysis similar to what we did in Sect. 9.3.4 yields four images:

$$(\theta_1,\theta_2) = \left(0\,,\ \pm\frac{\theta_E}{1-\gamma}\right) \quad \text{and} \quad (\theta_1,\theta_2) = \left(\pm\frac{\theta_E}{1+\gamma}\,,\ 0\right)$$

A source on the horizontal axis can be treated analytically as well. In Problem 9.6 you can find the following results:

- For $0 \le \beta_1 < 2\gamma\theta_E/(1-\gamma)$ there are four images. Two are on the θ_1-axis and two are off the axis.
- For $2\gamma\theta_E/(1-\gamma) < \beta_1 < \theta_E$ there are two images, both on the θ_1-axis.

This helps you understand the different configurations seen in Fig. 9.4, as well as the transition between two and four images. There is one additional type of 4-image configuration that is produced by an off-axis source, but it is usually found numerically.

We have considered ellipticity *or* shear, but real lenses may have both. Quantitatively, both ellipticity and shear are often required to fit observed 4-image lenses in detail. Qualitatively, though, the two models we have considered capture the main phenomenology of 4-image lensing.

9.3.6 Science with Galaxy Strong Lensing

Several hundred cases of strong lensing by galaxies have now been observed; in some the source is a quasar or other compact source that is lensed into multiple distinct images, while in others the source is a galaxy that is lensed into a partial or complete Einstein ring. The majority of lens galaxies are ellipticals because such galaxies tend to be more massive, and hence better lenses, than spirals.

So far in this chapter we have assumed a mass distribution and solved for the image positions. When we study observed lenses, we invert the problem: we take

[11] "External" because it comes from outside the main lens galaxy (i.e., from the neighbors). Note that we drop the subscript on γ to simplify the notation.

the images as given and try to solve for the mass distribution that produced them. It impossible to uniquely determine the mass distribution, though; there are just too many unknowns. To make progress, we often adopt assumptions that limit the unknowns.[12] For example, if we assume the lens is a point mass or singular isothermal sphere then we only need to solve for the mass or velocity dispersion (respectively). We can make the model more complicated by adding more parameters: for example, moving from an isothermal profile to a general power law adds one parameter; allowing the mass distribution to be elongated adds two (ellipticity and orientation angle); accounting for external shear adds another two (shear strength and direction); and so forth. A lot of the art and science of strong lens modeling lies in choosing assumptions whose restrictions are useful but not oversimplified, incorporating observational and/or theoretical knowledge from other realms of astrophysics.

Strong lens modeling has taught us a number of lessons about galaxy mass distributions (see the review by Treu [18]; you can explore some aspects of lens modeling in Problem 9.7). The most robust quantity we can measure is the mass within the Einstein radius, $M(\theta_E)$. By comparing the mass inferred from lensing with the mass associated with the starlight, we can find evidence that lens galaxies contain dark matter. The next step is to learn how the dark matter is distributed. One approach is to recognize that θ_E varies from one lens to another (it depends not only on the lens mass but also on the distances between the observer, lens, and source); if we assume lenses follow certain scaling relations, we can use the various $M(\theta_E)$ measurements to infer the average mass profile. Another approach is to combine lensing with an analysis of stellar dynamics, which tends to be sensitive to the mass closer to the center of a galaxy (see Sect. 8.2.3). Having mass measurements at small radii from dynamics and somewhat larger radii from lensing provides important information about the mass profile in individual systems. All told, models suggest that lens mass distributions are nearly isothermal, so the dark matter halos are more extended than the visible galaxies.

We noted above that many lens models require both ellipticity and external shear. Constraints on shear let us investigate the distribution of matter in the vicinity of a lens, which is interesting because lens galaxies often lie in gravitationally bound "groups" containing a few dozen galaxies [19]. Lensing therefore helps us study how galaxies form and evolve in environments that play an important role in galaxy evolution.

[12] An alternative approach is to make as few assumptions as possible (although assumptions can never be avoided altogether), and then deal with the large range of mass models that are consistent with the observed images [17].

9.4 Weak Lensing

To this point we have considered situations in which the impact parameter is small and light bending is strong enough to create multiple images. At larger impact parameters, lensing still acts but the effects are more subtle. Consider an array of source galaxies as shown in the left panel of Fig. 9.12. Putting a lens in front yields the picture shown on the right. Only sources near the center are multiply imaged, but sources farther out are still distorted. This is the regime known as **weak lensing**.

There is not much we can learn from *individual* sources that are weakly lensed. The observed shape of an image depends not only on the lensing distortion but also on the intrinsic shape of the source, and it is difficult or impossible to distinguish the two effects on a galaxy-by-galaxy basis (see Fig. 9.13). We can make progress, though, by examining *collections* of galaxies. Weak lensing distortion is predominantly tangential (perfectly so in the case of a spherical lens), whereas intrinsic shapes and orientations are random.[13] Therefore if we measure the shapes of galaxies in polar coordinates centered on a lens, the intrinsic shapes should average out while the lensing distortions will not.

One way to study weak lensing is to collect galaxies into annuli centered on the lens, compute the average shape in each annulus, and relate that to the lensing shear. As you can show in Problem 9.2, the shear is related to the density for a circular lens by

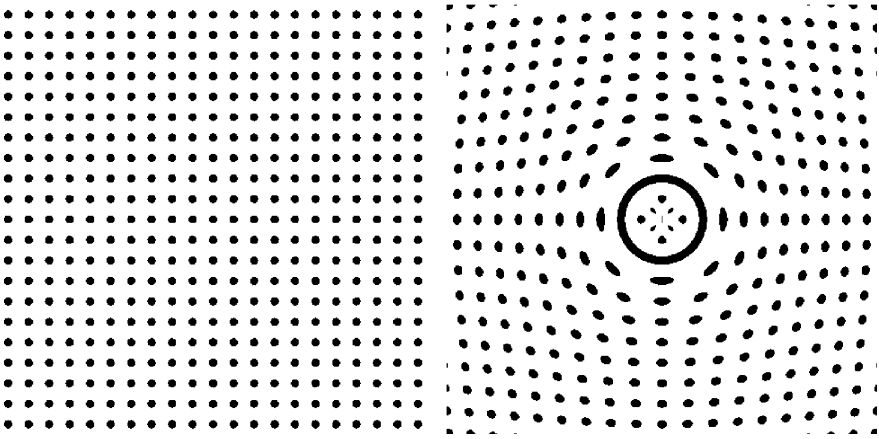

Fig. 9.12 The *left panel* shows an array of source galaxies. The *right panel* shows what we would see if there were a gravitational lens in front. One source produces an Einstein ring, a few are multiply imaged, but most are only slightly distorted ("weak lensing")

[13] We hope. Correlations among the intrinsic shapes of galaxies could present a challenge for weak lensing [20, 21], but they are generally expected to be small and there are ways to deal with them in a weak lensing analysis [22].

Fig. 9.13 Similar to Fig. 9.12, but the source galaxies have random positions, shapes, and orientations. The images are no longer perfectly tangential, but the overall pattern of distortion is still apparent

$$\gamma(r) = \frac{\bar{\Sigma}(r) - \Sigma(r)}{\Sigma_{\rm crit}} \tag{9.28}$$

where $\bar{\Sigma}(r)$ is the average surface mass density within radius r. Measuring the shear profile clearly provides information about the density profile of the lens.

A more sophisticated approach is to observe a large sample of galaxies, collect them in bunches on the sky, and measure the full shear map (at a spatial resolution that is limited by the sample size). If we know both γ_+ and $\gamma_\times$ as a function of position, we can view Eqs. (9.13b) and (9.13c) as a pair of differential equations that can be solved for the lens potential, ψ. We can then use Eq. (9.21) to uncover the underlying mass distribution, Σ. This general analysis cannot be done analytically, but it is well suited to computational methods (e.g., [23]).

The challenge of weak lensing is that its statistical nature provides less detailed information about lens mass distributions, compared with strong lensing. The benefit is that there are many, many more objects in the universe that are weakly lensed than objects that are strongly lensed. As a result, weak lensing has become a widespread and important tool for studying dark matter. This is especially true for clusters of galaxies, which are the most massive bound objects in the universe and thus good targets for weak lensing (see the review by Kneib and Natarajan [24]).

Figure 9.14 shows a famous weak lensing system known as the "bullet cluster," which provides arguably the clearest evidence that dark matter is real. The system contains two clusters of galaxies that passed through each other some 100 million years ago; the cluster on the left is moving to the left, and the one on the right is moving to the right. Each cluster contained hot gas that can be mapped because it

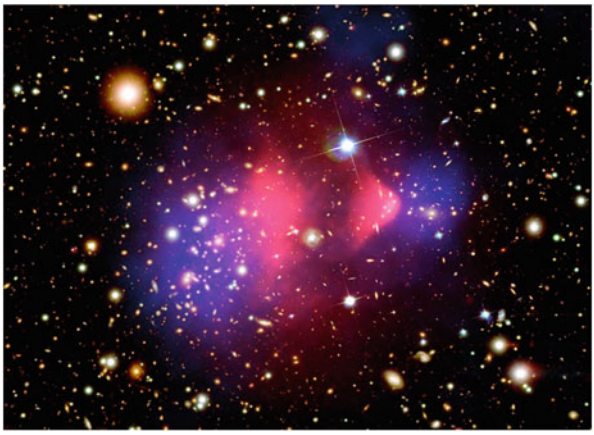

Fig. 9.14 Composite image of the "bullet cluster" system. Superposed on an image of the galaxies is a map of the hot X-ray gas (*colored red*) and the dark matter inferred from weak lensing (*colored blue*) (Credit: X-ray: NASA/CXC/M. Markevitch et al. Optical: NASA/STScI; Magellan/U. Arizona/D. Clowe et al. Lensing Map: NASA/STScI; ESO WFI; Magellan/U.Arizona/D. Clowe et al.)

emits X-rays (colored red in the image). During the "collision" the two gas clouds slammed into one another, but the galaxies and dark matter did not feel gas pressure so they kept on going. As a result, the X-ray gas got separated from the galaxies and dark matter.

How does lensing apply? There are lots and lots of small background galaxies in the field (although they are too small and faint to be apparent in Fig. 9.14). A weak lensing analysis yields the mass distributions indicated in blue in the image [25]. There is a significant offset between the hot gas, which represents the bulk of the normal matter in the clusters, and the source of gravity. This is exactly what we would expect if there is a significant amount of dark matter that exerts gravity but is otherwise inactive. Most astrophysicists conclude that it would be very difficult to explain the weak lensing result in the bullet cluster and similar systems [26] without exotic dark matter (but see [27] for a dissenting view).

Strong and weak lensing are most apparent near massive objects like galaxies and clusters, but gravitational deflection actually affects all light rays in the universe at some level. Inhomogeneities in the large-scale distribution of matter create distortions that are quite small but detectable with a careful statistical analysis of galaxy shapes [28]. This **cosmic shear** is sensitive to the relative abundances of dark matter and dark energy in the universe, so it plays a prominent role in existing and planned probes of cosmology [29]. The analysis methods are more detailed than we want to get into here, but the fundamental principle is just what we have used throughout this chapter: mass creates gravity that bends light, so if we can detect the light bending we can use it to map the matter and weigh the universe.

Problems

9.1. This problem will help you understand the interpretation of κ, γ_+, and $\gamma_\times$ in Eq. (9.12). Let the source be a unit circle and write its boundary as

$$\Delta\boldsymbol{\beta} = (\cos\phi, \sin\phi)$$

where ϕ is an azimuthal angle running from 0 to 2π. Use Eq. (9.10) to find and plot the boundary of the image for the following cases:

(a) $\kappa = 0.2$ and $\gamma_+ = \gamma_\times = 0$
(b) $\gamma_+ = \pm 0.2$ and $\kappa = \gamma_\times = 0$
(c) $\gamma_\times = \pm 0.2$ and $\kappa = \gamma_+ = 0$

9.2. In this problem we consider the lensing properties of a circular mass distribution. In the text we refer to the two components of position on the sky as (θ_1, θ_2), but for the sake of familiarity let's revert to (x, y) and the associated polar coordinates (r, ϕ). With circular symmetry, the lens potential is a function of r only: $\psi(r)$.

(a) Work out the first and second derivatives of the potential with respect to x and y, but expressed in polar coordinates. For example, the chain rule for derivatives gives

$$\frac{\partial\psi}{\partial x} = \frac{\partial r}{\partial x}\psi'(r) + \frac{\partial r}{\partial y}\psi'(r)$$

where $\psi'(r) = \mathrm{d}\psi/\mathrm{d}r$.

(b) Use Eq. (9.13) to show that the convergence and shear can be written as

$$\kappa = \frac{1}{2}\left(\frac{\psi'}{r} + \psi''\right) \tag{9.29a}$$

$$\gamma_+ = \frac{1}{2}\left(\frac{\psi'}{r} - \psi''\right)\cos 2\phi \tag{9.29b}$$

$$\gamma_- = \frac{1}{2}\left(\frac{\psi'}{r} - \psi''\right)\sin 2\phi \tag{9.29c}$$

where $\psi'' = \mathrm{d}^2\psi/\mathrm{d}r^2$.

(c) In circular symmetry, the deflection is $\alpha = \psi'$. Use this with Eq. (9.29) to show that the magnification has the form given in Eq. (9.16)

(d) From Eqs. (9.29b) and (9.29c) it is clear that the shear strength is

$$\gamma = \frac{1}{2}\left(\frac{\psi'}{r} - \psi''\right)$$

Now derive Eq. (9.28). You will need to use Eqs. (9.20), (9.22), and (9.23).

9.3. Consider a star orbiting 10 pc from the black hole at the center of the Milky Way (see Sect. 3.2.1). Suppose we view the star's orbit perfectly edge-on.

(a) What is the Einstein radius for this scenario (in arcsec)?
(b) When the star is at a source angle of $\beta = 0.1''$, where are the two gravitationally lensed images?
(c) When the star passes behind the black hole we see a "microlensing" event. How long does it last?
(d) If the star's orbit were larger, how would the answers change? Explain using equations or drawings.

9.4. Let's see how to calculate points on a microlensing light curve. In the figure below, the line denotes the trajectory of a source passing behind a point mass lens. The circle indicates the Einstein radius. All lengths are in units of the Einstein radius. For each of the three marked source positions, find the two images, compute their individual magnifications, and then find the total magnification is $\mu_{\rm tot} = |\mu_+| + |\mu_-|$ (with absolute values because in this problem we do not worry about parities).

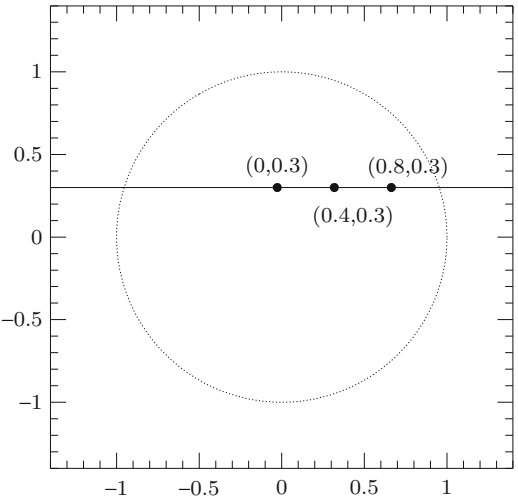

9.5. As discussed in Sect. 9.2, microlensing is used to test the hypothesis that the Milky Way's dark matter is made of MACHOs. In this problem you will estimate the microlensing probability. (This is analogous to Problem 8.4, with the interloper star replaced by a light ray.)

(a) Suppose there is a uniform mass density ρ in MACHOs between us and a source a distance D_s away. Consider a thin slab that is located a distance D_l away and has thickness $\mathrm{d}D_l$. Find the fraction of the area of the slab that is covered by the Einstein rings of MACHOs. This is the probability that the light ray passes within one Einstein radius of one of the MACHOs in the slab, i.e., close enough to be strongly lensed. Hints: θ_E is the angular Einstein radius, but here you need to convert it to a length; the result does not depend on the mass of the MACHOs.

(b) Now sum up all the slabs between us and the source, i.e., integrate over D_l. The resulting quantity is called the "optical depth" for microlensing, often written as τ, and it represents the probability that a light ray passes close enough to a MACHO to be lensed.
(c) To compute a numerical value of τ you need to specify the mass density in MACHOs. To make a simple estimate, assume that dark matter is distributed uniformly between the Sun and the center of the Milky Way, and compute the mean density. Also assume that all of the mass is in MACHOs (i.e., don't worry about the disk). With these assumptions, calculate ρ.
(d) Now compute the probability that a star at the center of the Milky Way is microlensed by a MACHO.

9.6. In this problem you will see why some lenses have two images and others have four. The simplest lens that can produce four images is an isothermal sphere with an external shear, whose lens equation is given by (9.27). Recall that γ is dimensionless, and we can take it to be positive.

(a) Consider a source placed on the horizontal axis in the source plane (i.e., $\beta_2 = 0$). Solve the lens equation (working with symbols) to show that:

- For $0 \leq \beta_1 < 2\gamma\theta_E/(1-\gamma)$ there are four images. Two are on the θ_1-axis and two are off the axis.
- For $2\gamma\theta_E/(1-\gamma) < \beta_1 < \theta_E$ there are two images, both on the θ_1-axis.

Give the positions of all images in both cases.
(b) Now assume $\theta_E = 1''$ and $\gamma = 0.1$, which are typical values for galaxy lenses. Sketch the image configurations for the following source positions:

- $\beta_1 = \beta_2 = 0$
- $\beta_1 = 0.15''$ and $\beta_2 = 0$
- $\beta_1 = 0.35''$ and $\beta_2 = 0$

9.7. This problem will give you a taste of how we model gravitational lens systems to measure galaxy masses. Imagine you observe a galaxy lens system with distances $D_l = 940\,\text{Mpc}$, $D_{ls} = 1{,}293\,\text{Mpc}$, and $D_s = 1{,}745\,\text{Mpc}$. One image appears at an angular position of $\theta_+ = 1.05''$ from the lens galaxy, while the other appears at an angular position $\theta_- = -0.35''$ on the opposite side of the galaxy. You may assume the lens is circularly symmetric.

(a) Assume the galaxy can be modeled as a point mass. Find the Einstein radius and mass of the lens galaxy.
(b) Now assume the galaxy can be modeled as an isothermal sphere. Again find the Einstein radius and the mass enclosed by the Einstein radius.
(c) Both models can fit the image positions, but they make different predictions for the brightnesses. Suppose the "+" image is observed to be three times brighter than the "−" image. Compute the relative magnifications of the images for your point mass and isothermal models. Which model is correct?

Hint: remember to convert between arcseconds and radians as necessary.

9.8. We know that black holes come in stellar-mass and supermassive varieties, but we do not know whether there is anything in between. In this problem we consider whether gravitational lensing could be used to look for intermediate mass black holes (IMBH) in globular clusters.

(a) Consider a globular cluster with mass $M_{\rm tot}$ and velocity dispersion σ. Assuming a uniform density of stars with mass m, use the virial theorem to estimate the size of the cluster and the number density of stars.
(b) Suppose there is an IMBH at the center of the cluster, and the mass is $M_\bullet$ such that $m \ll M_\bullet \ll M_{\rm tot}$. The black hole can lens background stars that are in its "Einstein cone"—the region behind the black hole whose projected radius equals the Einstein radius.[14] Find an approximate expression for the size of the Einstein cone as a function of D_{ls}. Hints: you may assume $D_l \approx D_s$ and $D_{ls} \ll D_s$; recall that Eq. (9.7) gives the Einstein radius in angular units.
(c) Estimate the total number of stars in the Einstein cone. This is the expected number of lens systems within the globular cluster. Hint: the answer can be expressed in terms of $M_\bullet$, m, and σ.
(d) Obtain a quantitative estimate for the number of lenses by assuming that the M-σ relation for supermassive black holes (Sect. 3.2.2) can be applied to globular clusters:

$$M_\bullet = 1.35 \times 10^8\, M_\odot \times \left(\frac{\sigma}{200\,{\rm km\,s^{-1}}}\right)^{4.02}$$

Use $\sigma \sim 10\,{\rm km\,s^{-1}}$ for a globular cluster.
(e) The same analysis can be applied to an SMBH in an elliptical galaxy. Repeat part (d) for a galaxy with $\sigma \sim 200\,{\rm km\,s^{-1}}$.
(f) Comment on our ability to detect and identify lensing of stars in a globular cluster or galaxy by a massive black hole *within* the stellar system.

9.9. Suppose you observe a binary star system consisting of a white dwarf with a radius of 6,100 km and a neutron star with a radius of 10 km. The system is 2 kpc from us and viewed edge-on. The radial velocity curves are shown below, where WD labels the white dwarf and NS labels the neutron star.

(a) What are the masses of the two stars, and the distance between them?
(b) Sketch the light curve when the neutron star passes behind the white dwarf. Hint: since the problem appears in this chapter, you can assume it involves gravitational lensing, but that is not the only phenomenon at work.

[14] This is not strictly a cone because the edge is not straight, but the terminology is helpful because the region does grow with distance behind the black hole.

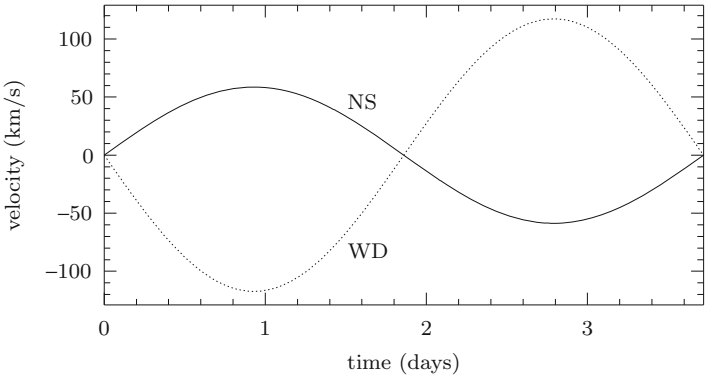

References

1. C.R. Keeton, A.O. Petters, Phys. Rev. D **72**(10), 104006 (2005)
2. V. Bozza, Gen. Relativ. Gravit. **42**, 2269 (2010)
3. F.W. Dyson, A.S. Eddington, C. Davidson, R. Soc. Lond. Philos. Trans. Ser. A **220**, 291 (1920)
4. W.W. Campbell, Publ. Astron. Soc. Pac. **35**, 11 (1923)
5. C.R. Keeton, S. Burles, P.L. Schechter, J. Wambsganss, Astrophys. J. **639**, 1 (2006)
6. S. Dong et al., Astrophys. J. **642**, 842 (2006)
7. A. Gould et al., Astrophys. J. **720**, 1073 (2010)
8. K. Griest, Astrophys. J. **366**, 412 (1991)
9. J.L. Feng, Ann. Rev. Astron. Astrophys. **48**, 495 (2010)
10. C. Alcock et al., Astrophys. J. **541**, 734 (2000)
11. C. Alcock et al., Astrophys. J. **542**, 281 (2000)
12. C. Alcock et al., Astrophys. J. **479**, 119 (1997)
13. D. Kubas et al., Astron. Astrophys. **435**, 941 (2005)
14. B.S. Gaudi, Ann. Rev. Astron. Astrophys. **50**, 411 (2012)
15. J.P. Beaulieu et al., Nature **439**, 437 (2006)
16. C.R. Keeton, C.S. Kochanek, Astrophys. J. **495**, 157 (1998)
17. P. Saha, L.L.R. Williams, Astron. J. **127**, 2604 (2004)
18. T. Treu, Ann. Rev. Astron. Astrophys. **48**, 87 (2010)
19. K.C. Wong, C.R. Keeton, K.A. Williams, I.G. Momcheva, A.I. Zabludoff, Astrophys. J. **726**, 84 (2011)
20. R.A.C. Croft, C.A. Metzler, Astrophys. J. **545**, 561 (2000)
21. A. Heavens, A. Refregier, C. Heymans, Mon. Not. R. Astron. Soc. **319**, 649 (2000)
22. J. Blazek, R. Mandelbaum, U. Seljak, R. Nakajima, J. Cosmol. Astropart. Phys. **5**, 041 (2012)
23. N. Kaiser, G. Squires, Astrophys. J. **404**, 441 (1993)
24. J.P. Kneib, P. Natarajan, Astron. Astrophys. Rev. **19**, 47 (2011)
25. D. Clowe, M. Bradač, A.H. Gonzalez, M. Markevitch, S.W. Randall, C. Jones, D. Zaritsky, Astrophys. J. Lett. **648**, L109 (2006)
26. M. Bradač, S.W. Allen, T. Treu, H. Ebeling, R. Massey, R.G. Morris, A. von der Linden, D. Applegate, Astrophys. J. **687**, 959 (2008)
27. B. Famaey, S.S. McGaugh, Living Rev. Relativ. **15**, 10 (2012)
28. A. Refregier, Ann. Rev. Astron. Astrophys. **41**, 645 (2003)
29. A. Albrecht et al., ArXiv e-prints arXiv:astro-ph/0609591 (2006)